Engineering Solutions to Mechanics, Marine Structures and Infrastructures

Eng. Solut. Mech. Mar. Struct. Infrastruct.
2024.1(4).10
ISSN：2960-0979
https://doi.org/10.58531/esmmsi/1/4/10

Article

Maritime Thermal Launch Rocket Exhaust Plume Impact on Surrounding Facilities

Ying Xue, Dapeng Zhang*

Ship and Maritime College, Guangdong Ocean University, Zhanjiang 524005, China
*Correspondence: Dapeng Zhang, zhangdapeng@gdou.edu.cn

Academic Editor: Weiwei Wang <zhwangww@ytu.edu.cn>
Received: 15 December 2024; Revised: 27 December 2024; Accepted: 29 December 2024; Published: 30 December 2024

Abstract: This study conducts in-depth research on the impact of rocket exhaust plumes on the marine environment and facilities during launch, offering a scientific foundation for thermal protection design of carrier rocket launch platforms. A dual-nozzle rocket engine exhaust plume model is developed to compute temperature and pressure distributions at various distances from sea level and the rocket center. Results indicate that gas temperatures decline slowly at higher altitudes, necessitating adequate protection for taller structures situated farther from the rocket. Structures within 1m to 5m of the rocket must endure significant temperature variations with height. This data serves as a reference for the safe design of maritime launch platforms.

Keywords: Rocket Exhaust Plume; Impact flow field; Surrounding facilities; Numerical simulation; Thermal protection design

1. Introduction

In recent years, the rapid advancement of aerospace technology has led to a surge in demand for space launch activities. Traditional land-based launch sites encounter numerous challenges in accommodating this growing demand. As an innovative launch approach, sea launch effectively tackles issues such as limited launch windows, intricate trajectory design, and debris fall zone safety, by leveraging its distance from populated areas and offering flexibility in selecting launch points and fall zones.

Citation: Xue Y., Zhang D. Maritime Thermal Launch Rocket Exhaust Plume Impact on Surrounding Facilities. Eng. Solut. Mech. Mar. Struct. Infrastruct., 2024, 1(4), doi: 10.58531/esmmsi/1/4/10

While sea launch platforms indeed mitigate the direct threat of rockets to land-based populations, the exhaust plume comprising high-temperature gases and debris can pose a risk to marine facilities and vessels. During rocket launch, the exhaust plume contains high-temperature gases, which, upon contact with marine facilities, may cause melting, deformation, or combustion dueto the extreme heat, thereby damaging the structure and functionality of the facilities. Notably, sea launches tend to exhibit greater instability compared to land launches, complicating the task of on-site personnel to evacuate promptly in the event of an accident. Consequently, the significance of conducting a thorough thermal environment analysis for carrier rocket launch platforms is further emphasized.

Numerous scholars have employed numerical simulation methods to studythe shock flow field of the combustion gas jet during the takeoff phase of carrier rockets[1-2]. Zhao et al. used numerical simulation to investigate the flow field and thermal environment of the launch platform during the takeoff phase of carrier rockets, exploring the impact of the jet on the launch platform, support arms, and cover plates, providing a reference for the safe design of carrier rocket launch platforms. Tsutsumi et al. conducted research on the impact of the layout of the first-stage rocket engines on the internal flow field of the launch pad using numerical simulation, discovering that the combustion gas jet of solid rocket boosters can interfere with the diffusion of the jet of liquid rocket engines on the diversion trench and lead to reverse jet flow[6]. Wang et al.compared the heat flux impact of single and dual nozzles on the ground based on numerical calculations, providing a data basis for rocket nozzle design[3]. Zhou et al. used numerical simulation to study the impact of the angle of the diversion trench on the exhaust direction performance during the launch phase of a four-nozzle carrier rocket, providing a reference for the design of diversion trenches[4]. Teng et al. established a numerical model for the exhaust jet of a four-nozzle rocket engine, clarifying the supersonic heat flux impact on the offshore support platform during the hot launch of carrier rockets, which has important reference value for the safe design of offshore launch support platforms and innovation in diversion structures during subsequent hot launches.

The aforementioned literature provides in-depth research data on the shock flow field of the combustion gas jet during the takeoff phase of carrier rockets. However, most of the literature focuses on the impact of rockets on launch platforms and the ground, with limited information on the impact of rocket exhaust plume shocks on surrounding facilities[5].

This paper presents a numerical simulation of the launch process of a specific dual-nozzle liquid carrier rocket, utilizing a grid count exceeding 1.56 million for enhanced precision. The study analyzes the surface temperature and pressure distributions of various objects situated at differing distances from the launch pad. The findings provide valuable insights for the thermal protection design of carrier rocket launch platforms.

2. Theoretical Basis

2.1 Basic Concepts of Combustion Jet

A combustion jet refers to the high-temperature, high-speed gas flow ejected from a rocket engine. During the rocket launch process, the combustion jet significantly impacts the surrounding environment, including changes in temperature, pressure, and the formation of flow fields. These factors are crucial for the safety design of the rocket launch platform and its surrounding facilities[2].

2.1.1 Formation of Combustion Jet:

The combustion jet is produced when fuel burns in the combustion chamber of a rocket engine, generating high-temperature, high-pressure gas that is expelled through the nozzle at high speed.

2.1.2 Role of Nozzle:

The design of the nozzle accelerates and expands the gas, forming a high-speed jet. The shape and size of the nozzle significantly influence the performance of the combustion jet. During operation, the high-temperature gas radiates heat to the nozzle's inner wall, and particles in the gas may contact and transfer heat, but these effects are negligible compared to convective heat transfer.

2.1.3 Energy Conversion:

The formation of the combustion jet involves energy conversion. The chemical energy released by fuel combustion is converted into thermal and kinetic energy of the gas, with kinetic energy being the primary form of energy that impacts the surrounding environment.

2.2 The combustion jet primarily consists of:

1.High-Temperature Gas: The main component of the combustion jet, produced by fuel combustion, characterized by high temperature and pressure.

2.Combustion Products: Including incompletely burned fuel, oxides generated by combustion, and other chemical reaction products.

3.Flowing Gas: Accelerated and expanded by the nozzle, forming a high-speed flowing gas jet.

These components collectively constitute the combustion jet, impacting the rocket launch platform and surrounding facilities.

2.3 Design Improvement Directions for Launch Platform

2.3.1 Stability and Safety:

The launch platform must remain stable during rocket launch, preventing overturning or movement due to the enormous thrust generated.

Design considerations include the platform's structural strength and stiffness to withstand dynamic loads and impacts during launch[7-10].
Safety is the primary principle of design, encompassing the prevention of accidents such as fires and explosions, and ensuring the safety of personnel and equipment.

2.3.2 Support and Guidance:

The launch platform must provide sufficient support area to stably support the rocket and bear its weight. A guidance system ensures the rocket rises along the predetermined trajectory during launch, preventing deviation due to factors such as wind.

2.3.3 Thermal Protection:

Effective thermal protection systems are required for the launch platform to shield them from high-temperature thermal radiation and impact damage during rocket launch.Thermal protection materials should exhibit excellent high-temperature resistance and thermal stability, while also resisting erosion and scouring by the combustion jet[11-14].

2.3.4 Flexibility and Adaptability:

The launch platform should possess flexible movement and positioning capabilities to adapt to different launch sites and missions.The platform's design should facilitate transportation, installation, and commissioning, enhancing launch efficiency and reducing costs.

2.3.5 Environmental Compatibility:

The design of the launch platform should consider environmental protection, minimizing the impact of the launch process on the environment.
The platform should be compatible with the rocket and other parts of the launch system to ensure the smooth progress of the entire launch process.

2.3.6 Numerical Simulation and Optimization:

Numerical simulation techniques are utilized for the design and optimization of the launch platform to predict and analyze key parameters such as flow fields and thermal environments during the rocket launch.
Feedback from simulation results aids in improving and optimizing the platform structure, thermal protection system, etc., enhancing the platform's overall performance and reliability[15-20].

3.Relevant basic theories

3.1 Continuity Equation:

Describe the principle of mass conservation in fluid flow. For gas jets, it can be expressed as the rate of change of mass within a fluid element equals the difference between the mass flow rates entering and leaving that element[21].

$$\frac{\partial \rho}{\partial t}+\frac{\partial}{\partial x_i}(\rho u_i)=0 \tag{1}$$

3.2 Momentum Equation:

Describe the change in momentum during fluid flow. For gas jets, it can be expressed as the rate of change of momentum within a fluid element equals the sum of the external forces acting on that element[21-30].

$$\frac{\partial}{\partial t}(\rho u_i)+\frac{\partial}{\partial x_j}(\rho u_i u_j)=-\frac{\partial p}{\partial x_i}+\frac{\partial}{\partial x_j}[\mu(\frac{\partial u_j}{\partial x_i}+\frac{\partial u_i}{\partial x_j})-\frac{2}{3}(\mu\frac{\partial u_j}{\partial x_j})\delta_{ij}]+\rho g_i \tag{2}$$

3.3 Energy Equation:

Describe the energy conversion and conservation during fluid flow. For gas jets, it can be expressed as the rate of change of internal energy within a fluid element equals the sum of heat transferred into the element and work done by external forces.

$$\begin{gathered}\frac{\partial}{\partial t}(\rho E)+\frac{\partial}{\partial x_i}(\rho u_i E)=-\frac{\partial}{\partial x_i}(p u_i)+\frac{\partial}{\partial x_i}(\lambda\frac{\partial T}{\partial x_i})+\frac{\partial}{\partial x_i}(u_j\tau_{ij}) \\ \rho=f(p,T)\end{gathered} \tag{3}$$

3.4 Turbulence Model Equations:

Such as the Realizable k-ε two-equation model, used to describe the characteristics of turbulent flow.

$$\frac{\partial(\rho k)}{\partial_t}+\frac{\partial(\rho k u_i)}{\partial x_i}=\frac{\partial}{\partial x_j}\left[(\mu+\frac{\mu_t}{\sigma_k})\frac{\partial k}{\partial x_j}\right]+G_k-\rho\varepsilon \tag{4}$$

The equations typically involve terms for mixture viscosity μ, production of turbulent kinetic energy G, and constants for the model σ=1.0 1.

$$\frac{\partial(\rho\varepsilon)}{\partial t}+\frac{\partial(\rho\varepsilon u_i)}{\partial x_i}=\frac{\partial\varepsilon}{\partial x_j}\left[(\mu+\frac{\mu_t}{\sigma_\varepsilon})\frac{\partial\varepsilon}{\partial x_j}\right]+\rho D_1 E\varepsilon-\rho D_2\frac{\varepsilon^2}{k+\sqrt{\upsilon\varepsilon}} \tag{5}$$

$\partial_\varepsilon = 1.2;\ D_1$=1.4; D_2=1.9

3.5 Bernoulli's Equation:

Describe the conservation of energy in fluid flow. Although primarily used for incompressible fluids, it can sometimes be used to approximate energy changes in gas jets.

$$p_1+\frac{1}{2}\rho v_1^2+\rho g h_1=p_2+\frac{1}{2}\rho v_2^2+\rho g h_2 \tag{6}$$

4. Computational Model and Method

4.1 Grid Model

To determine when the rocket engine exhaust plume has the greatest impact on the surface, a simple 2D model was first established to simulate the rocket launch process. The results show that the rocket engine exhaust plume forms a relatively stable airflow on the surface after 0.4 seconds. The airflow velocity changes slowly at first, then quickly, and finally slows down again. At 1 second, the rocket engine exhaust plume has a relatively faster velocity and greater impact at approximately 20m above the ground. By consulting literature and referencing the numerical simulation method used by Zhao et al. to study the flow field and thermal environment of the launch platform during the carrier rocket's takeoff phase, the validity of the data was confirmed.

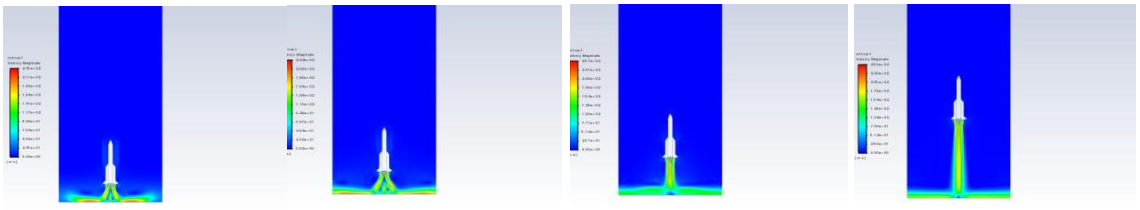

Figure 1. Flow field diagram of rocket takeoff process

Next, a 3D numerical model was constructed for a dual-nozzle rocket engine, referencing the method used by Teng et al. in "Numerical Simulation of Exhaust Plume of Four-Nozzle Carrier Rocket in Maritime Thermal Launch Mode". The nozzle performance was based on the performance of an ideal nozzle. An ideal nozzle is a one-dimensional nozzle where the exit pressure equals the ambient pressure, capable of producing the maximum thrust under design conditions. Its thrust coefficient is expressed as[38] .

$$CF=\sqrt{\frac{2k^2}{k\text{-}1}\left(\frac{2}{k+1}\right)^{\frac{k+1}{k-1}}\left[1-\left(\frac{pc}{pe}\right)^{\frac{k-1}{k}}\right]} \tag{7}$$

The nozzle throat diameter d is 300 mm, the nozzle expansion half angle is about 10 °, and the nozzle exit inner diameter is 1 000 mm. The rocket lift-off process was simulated by setting the center distance of the nozzle on the object as 20 m. The figure shows the geometric model of the nozzle of the dual-nozzle rocket engine.

Taking China's first maritime multi-functional vessel for aerospace launch and recovery, the Dongfang Hangtian Gang, as an example, its length is 162.5 meters and its width is 40 meters. Therefore, taking half the length of the ship, the atmospheric calculation domain was set as a cylinder with a radius of 80m and a height of 25m.

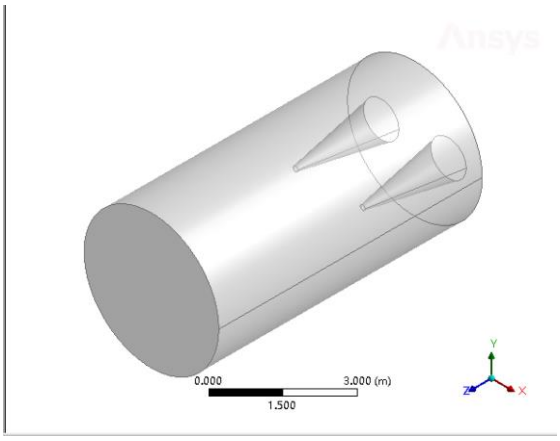

Figure 2. Geometric model of Dual-Nozzle rocket engine

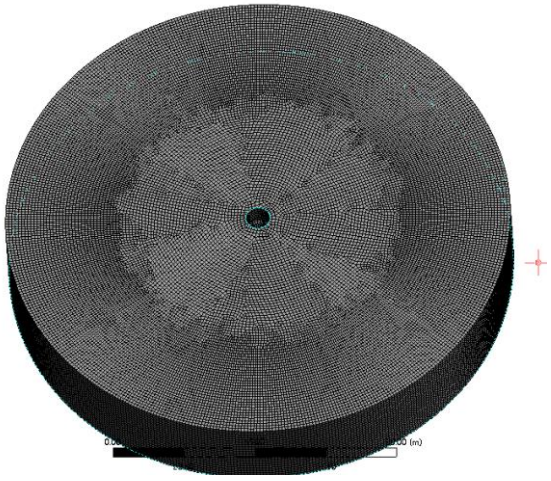

Figure 3. Fluid domain grid model

4.2 Simulation Boundary Conditions

During the simulation, it was assumed that the gas generated strictly follows the ideal gas state equation and undergoes an ideal state without heat exchange during the combustion process. The inner wall surface of the nozzle was insulated. Furthermore, the flow of fuel gas within the nozzle was considered an isentropic process, meaning the entropy of the fluid remains constant during the flow process.

The nozzle inlet was set as a pressure inlet type, with the total pressure at the inlet being 7MPa and the total temperature reaching 3000K. The incoming flow direction was perpendicular to the inlet boundary of the nozzle. The outlet was set as a pressure outlet boundary condition, with the ambient temperature at the outlet set to 300K and the air pressure set to atmospheric pressure. Finally, the nozzle itself and other related boundaries were set as no-slip and adiabatic wall boundary conditions to ensure the accuracy and consistency of the calculations[17].

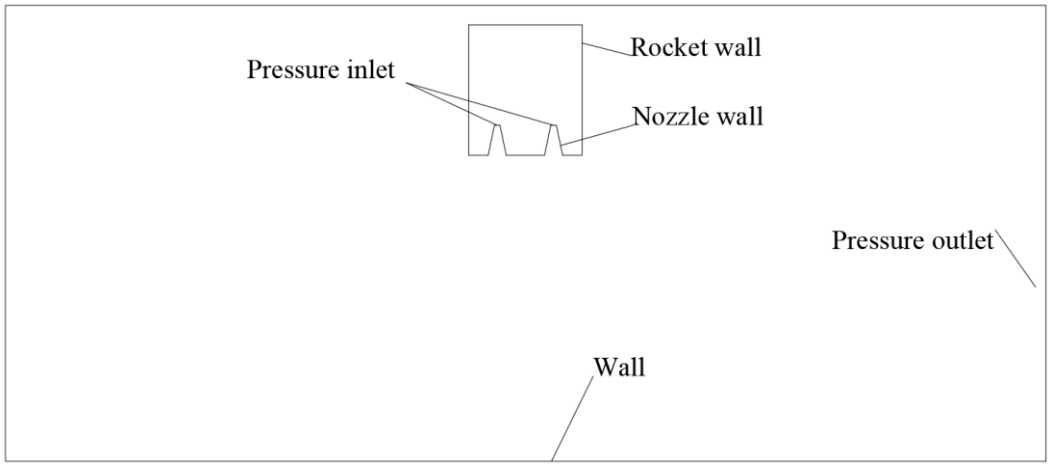

Figure 4. Model and boundary example

4.3 Numerical Simulation

Since the rocket propellant jet satisfies the continuum medium assumption and the ideal gas state equation, and there are no chemical reactions within the propellant jet, the Realizable k-ε two-equation turbulence model was adopted. The turbulent kinetic energy k equation is:

$$\frac{\partial（\rho k）}{\partial_t}+\frac{\partial（\rho k u_t）}{\partial x_i}=\frac{\partial}{\partial x_j}\left[（\mu+\frac{\mu_t}{\sigma_k}）\frac{\partial \kappa}{\partial x_j}\right]+G_\kappa-\rho\varepsilon \tag{8}$$

where μ is the mixture viscosity, G is the generation term of turbulent kinetic energy k caused by the average velocity gradient, and the constant coefficient σ = 1.0.

The turbulent kinetic energy dissipation rate ε equation is:

$$\frac{\partial（\rho\varepsilon）}{\partial t}+\frac{\partial（\rho\varepsilon u_i）}{\partial x_i}=\frac{\partial\varepsilon}{\partial x_j}\left[（\mu+\frac{\mu_t}{\sigma_\varepsilon}）\frac{\partial\varepsilon}{\partial x_j}\right]+\rho D_1 E\varepsilon-\rho D_2\frac{\varepsilon^2}{k+\sqrt{\upsilon\varepsilon}} \tag{9}$$

E representing the average characteristic strain rate.

The molar specific heat at constant pressure for each component in the atmospheric calculation domain is often calculated using a polynomial fitted from the JANNAF table.

$$\frac{cp_i}{Ru}=a_i^0+a_i^1T+a_i^2T^2+a_i^3T^3+a_i^4T^4 \tag{10}$$

The energy equation is:

$$h+\frac{u^2+v^2}{2}=h_0 \tag{11}$$

Due to computational power limitations, monitoring points were only placed at distances of 20m, 50m, and 70m from the rocket center, and at altitudes of 1m, 5m, and 10m.

5. Results

5.1 Temperature Changes at Different Heights

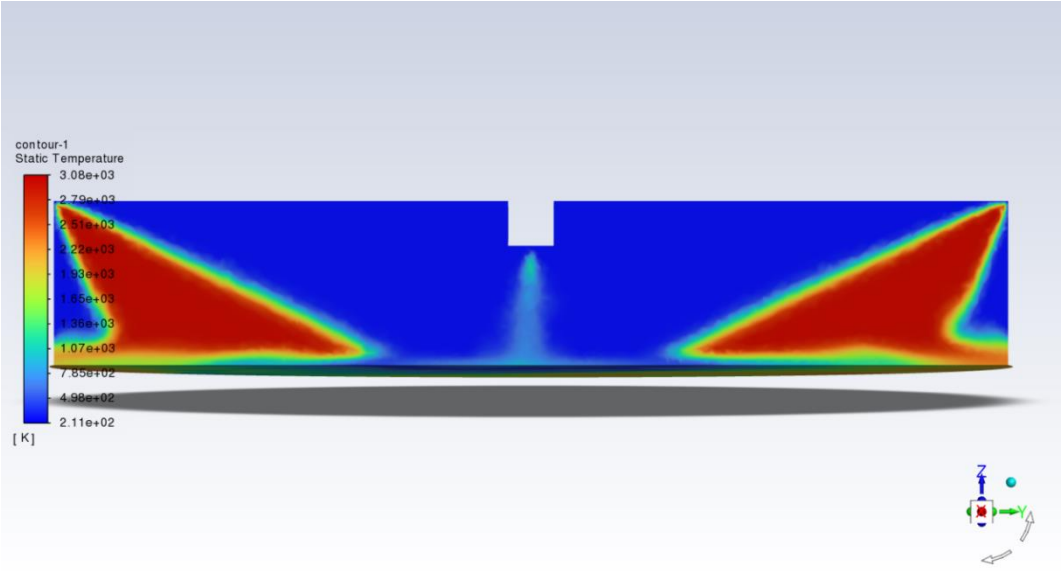

Figure 5. Fluid domain temperature change nephogram

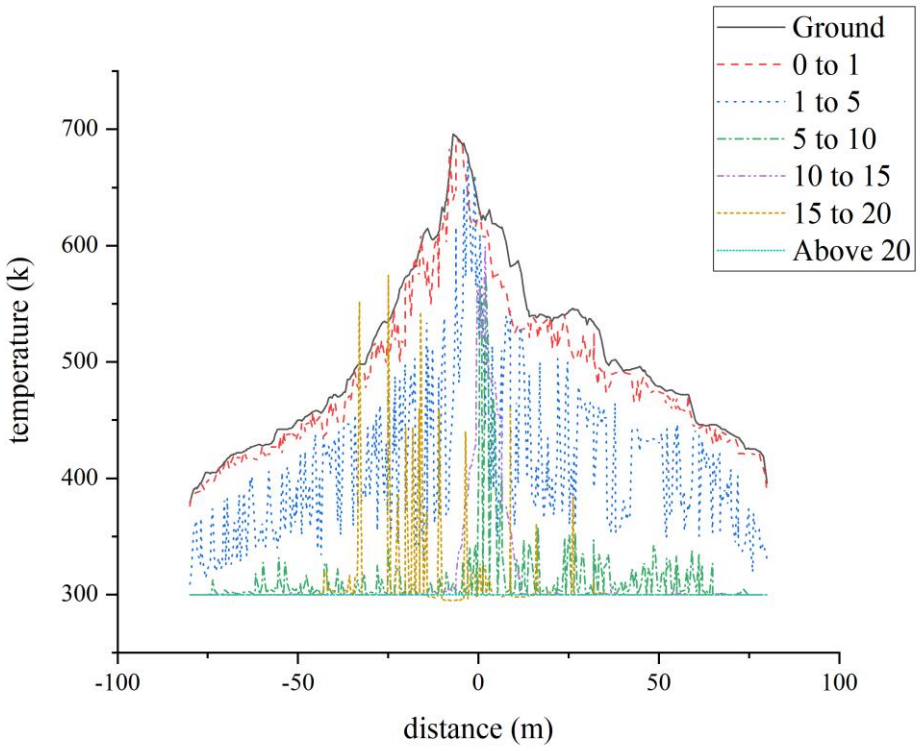

Figure 6. Temperature variation at different altitudes

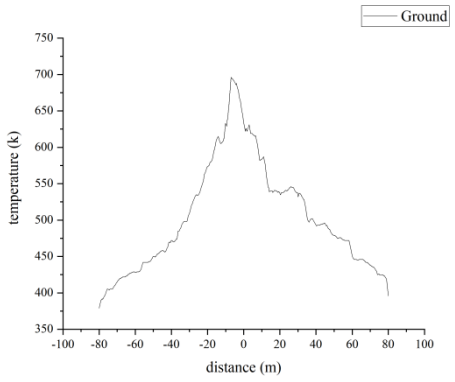

Ground

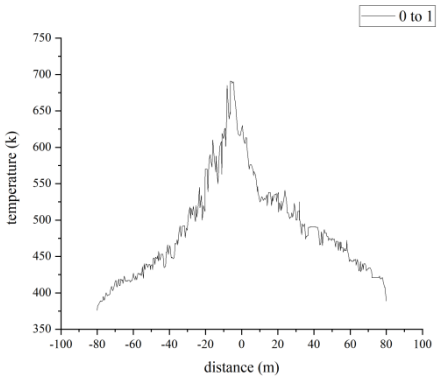

0 to 1

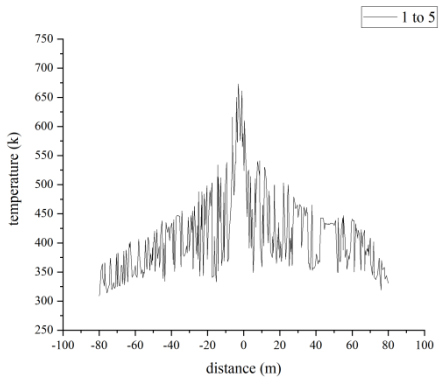

1 to 5

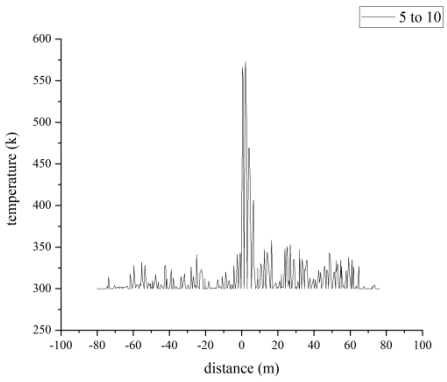

5 to 10

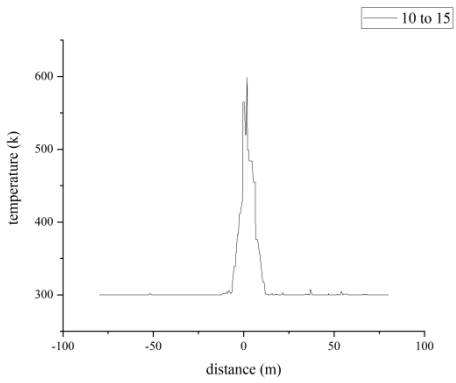

10 to 15

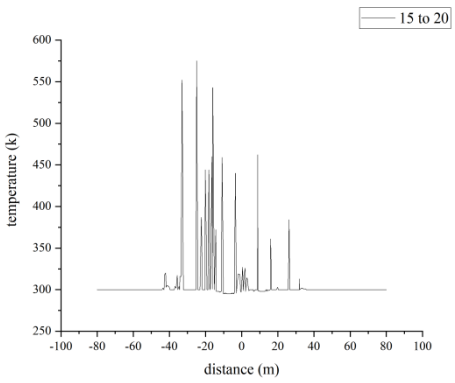

15 to 20

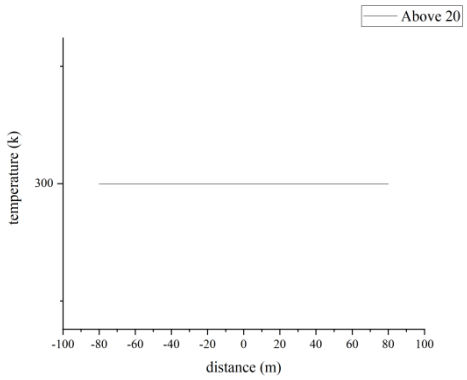

Above 20

Figure 7. Temperature variation at different altitudes

It can be seen from the graph that, in general, the temperature decreases as the distance increases. Specifically, at a distance of 1 m, the temperature starts at 800 K and gradually decreases to around 300 K with increasing distance. However, when the distance is 5 meters and 10 meters, the temperature drop trend is slightly different. At 5 meters above the ground, the temperature showed a trend of rising first, then falling and then rising; at 10 meters above the ground, the temperature changed slightly and rose slightly. And the air temperature at the three heights is gradually approaching. Therefore, it is speculated that the rocket engine wake is at a distance from the fire.Far away from the arrow, the thermal radiation to the air above is more obvious.

Vertical comparison of the temperature at different heights at the same distance shows that at 20 meters, the temperature at each altitude is higher and changes fastest with the altitude. It shows that in the place close to the rocket, the building should be made of materials with good high temperature resistance and extremely high thermal stability.

5.2 Pressure Changes at Different Heights

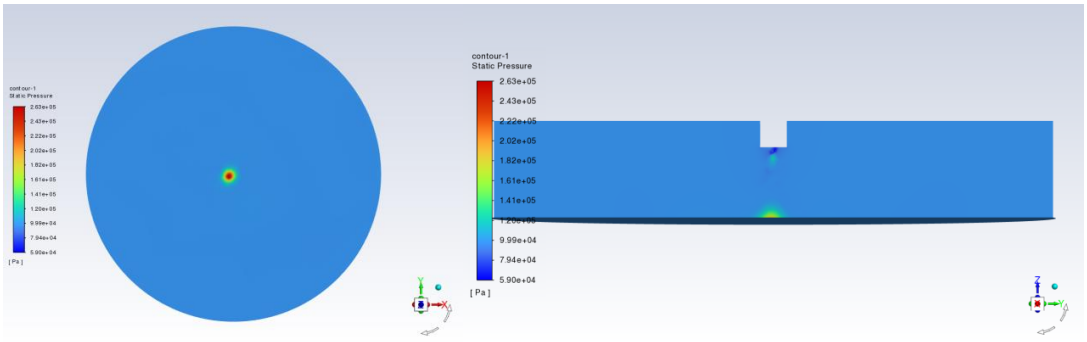

Figure 8. Fluid domain pressure variation nephogram

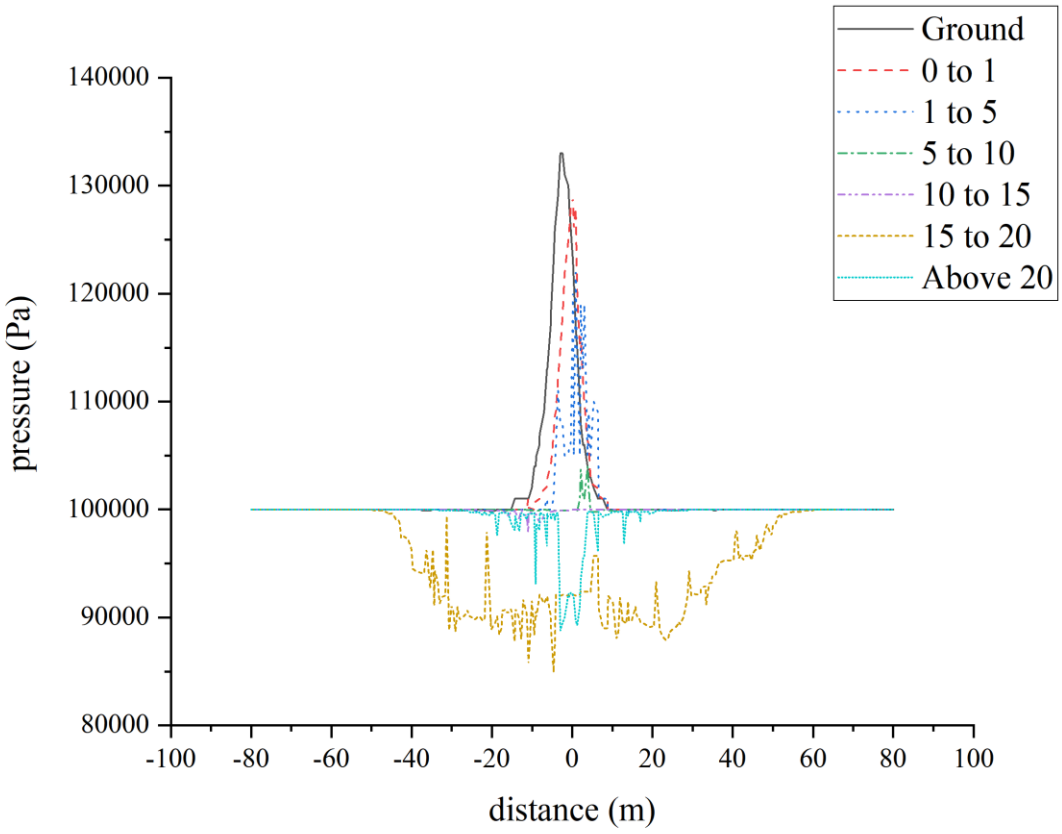

Figure 9. Pressure variation at different altitudes

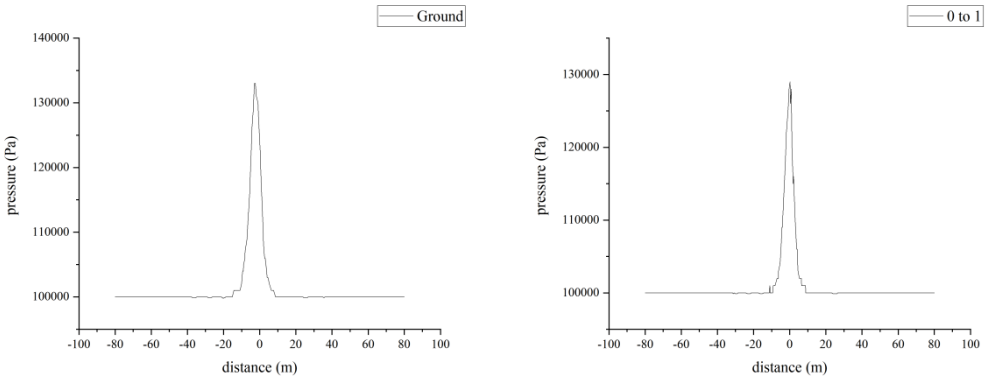

Ground **0 to 1**

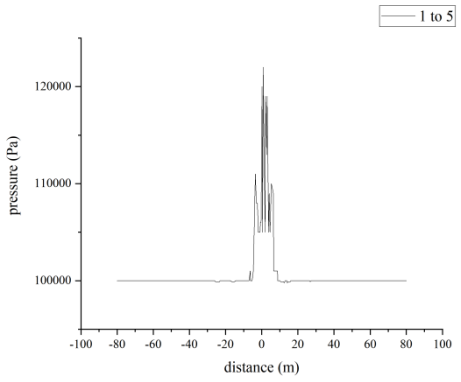

1 to 5

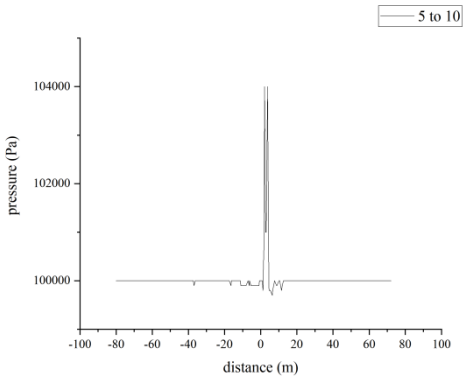

5 to 10

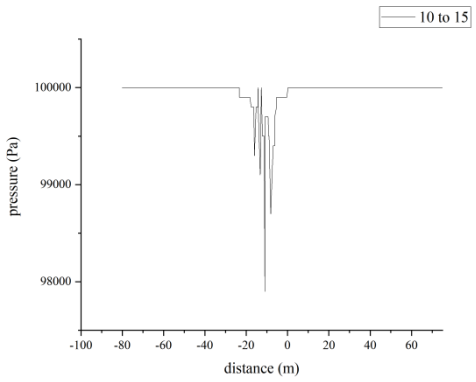

10 to 15

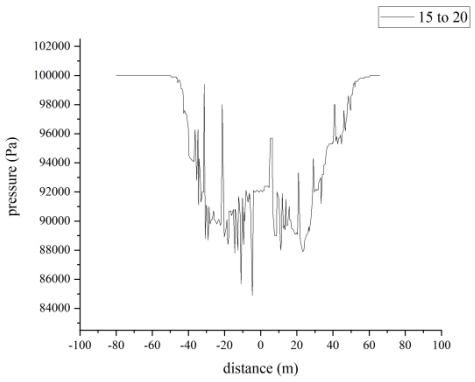

15 to 20

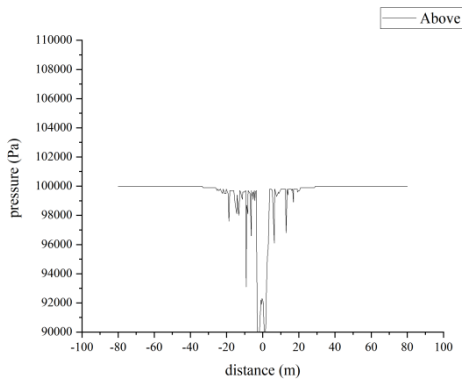

Above 20

Figure 10. Pressure variation at different altitudes

As can be seen from the chart, when the engine is operating, the pressure is only greater below the rocket, about 10 meters from the center, and is similar to the atmospheric pressure elsewhere. Ten meters away, with the increase of the distance, except for the higher height from the ground (such as 10 m), the pressure first decreases and then increases, and the pressure generally shows a trend of first increasing, then decreasing and then increasing. When the distance is close, the pressure gradually increases, reaches a peak value and then begins to decrease. This change pattern of first rising and then falling is reflected in different distances. From the analysis, it can be seen that in the case of higher height from the groundIn this case, the air pressure is not easy to be affected by the rocket gas when the distance is close, but the air pressure at different heights shows an upward trend when the distance is far (such as 50m to 70m), but the change is small, and the difference between the air pressure and the atmospheric pressure is not large.

Vertically comparing the air pressure at different heights at the same distance, it can be seen that the air pressure shows a counter-intuitive low value at a closer distance from the rocket, and the lower the altitude, the more obvious the situation. Compared with the temperature change table, it is speculated that at 10m, the gas temperature is higher, the density is lower, the external expansion work is done, and the air pressure is lower; at 20m, when the gas atmospheric pressure produces resistance to the jet

As the jet advances, this resistance gradually increases, resulting in a decrease in flow velocity, and the kinetic energy is gradually converted into other forms of energy, such as heat, with the temperature and pressure peaking at 20 meters34. At 50 meters, the temperature decreases, the gas density gradually increases, and the pressure gradually returns to atmospheric pressure.

6. Conclusions

1) The rocket engine exhaust plume has a more pronounced thermal radiation effect on the air above it at farther distances from the rocket. The temperature drops significantly when the distance exceeds ten meters, but the gas temperature decreases slowly at higher altitudes, and taller structures farther from the rocket still require adequate protection.The understanding that the rocket engine exhaust plume has a pronounced thermal radiation effect at farther distances, especially at higher altitudes, necessitates enhanced thermal management strategies.

2) In the vicinity of the rocket, buildings should use materials with good high-temperature resistance and high thermal stability to cope with drastic temperature changes with height.This will influence the choice of building materials and components in launch facilities and surrounding structures, ensuring they can maintain structural integrity and operational functionality under extreme temperature conditions.

3) Pressure and high-temperature protection indices need to be significantly increased within ten meters of the rocket. Beyond fifty meters, pressure gradually returns to atmospheric pressure, and temperature gradually returns to room temperature, allowing for a significant reduction in protection standards.

4) Future designs should incorporate materials and technologies that can effectively shield taller structures and sensitive equipment from the high temperatures and thermal radiation of the rocket plume, even at considerable distances.Structures near rocket launch sites will be designed with optimized layouts and materials to minimize exposure to thermal radiation and high temperatures.

5) Future designs and practices will likely adopt zone-based approaches, with heightened protection measures in close proximity to the rocket and progressively lower standards as the distance increases.Cost-Effective Safety Measures: By adopting zone-based protection standards, designers can allocate resources more efficiently, implementing higher levels of protection where needed while reducing costs in areas where lower protection standards suffice.

Acknowledgments: I am very sincerely grateful to the correspondence Dr. Dapeng Zhang for his guidance and direction of my research.

Funding: This work was financially supported by Program for Scientific Research Start-up Funds of Guangdong Ocean University(grant number 060302112008).

Conflict of interest: The authors of the article have consulted with each other and have no conflict of interest.

References:

1. Zhou Z, Zhang L, Le G. Numerical study for the flame deflector design of four-engine liquid rockets. Engineering Applications of Computational Fluid Mechanics, 2020;14(1): 726-737.
2. Zhou Siyin, Liu Xiang, Nie Wansheng, et al..Comparison of the effect of different external electrodes on discharge plasma-assisted diffusion flame stabilization.Plasma Science and Technology,2024;26(10):128-137.
3. Lee K S, Hong S K, Park S O. Supersonic jet im**ement Navier-Stokes computations for vertical launching system design applications. Journal of spacecraft and rockets, 2004;41(5): 735-744.
4. Liu Xinlin, Sun Jun, Jiang Zhuohang, et al. Study on Film/Regenerative Combined Cooling Characteristics of Liquid Oxygen/Methane Rocket Engine.Journal of Zhejiang University-Science A(Applied Physics & Engineering),2024;25(08):631-650.
5. Tsutsumi S, Sarae W, Ueda H, et al. Effect of rocket engine layouts on jet flowfield inside a launch pad. Journal of Spacecraft and Rockets, 2018; 55(6): 1537-1544.
6. u C, Zhou Z, Liang X, et al. Thermal environment of launch pads during rocket launching. Journal of Spacecraft and Rockets, 2022; 59(2): 489-496.
7. i J, Jiang Y, Yu S, et al. Cooling effect of water injection on a high-temperature supersonic jet. Energies, 2015;8(11): 13194-13210.
8. Andrews Jr E H, Craidon C B, Dennard J S, et al. Comparisons of Experimental Free-jet Boundaries with Theoretical Results Obtained with the Method of Characteristics. 1964.
9. LEWIS JR C H, CARLSON D J. Normal shock location in underexpanded gas and

gas-particle jets. AIAA Journal, 1964; 2(4): 776-777.
10. MacCormack R W. The effect of viscosity in hypervelocity impact cratering. Journal of spacecraft and rockets, 2003; 40(5): 757-763.
11. Abbett M. Mach disk in underexpanded exhaust plumes. AIAA Journal, 1971; 9(3): 512-514.
12. Bentin S, Gordon H W. Assessment of cognitive asymmetries in brain-damaged and normal subjects: validation of a test battery. Journal of Neurology, Neurosurgery & Psychiatry, 1979; 42(8): 715-723.
13. Kim K H, Chang K S. Axisymmetric im**ement of a hot jet on a flat plate: equilibrium flow analysis of high-temperature air. Shock Waves, 1994; 4: 155-162.
14. Keener E R, Spaid F W. Hypersonic nozzle-afterbody experiment-flow visualization and boundary-layer measurements. Journal of spacecraft and rockets, 1996;33(3): 326-332.
15. Alvi F, Iyer K. Mean and unsteady flowfield properties of supersonic im**ing jets with lift plates//5th AIAA/CEAS aeroacoustics conference and exhibit. 1999; 1829.
16. Saha S, Rathod S, Murty M S R C, et al. Numerical simulation of base flow of a long range flight vehicle. Acta Astronautica, 2012;74: 112-119.
17. Oh H, Lee J, Um H, et al. Numerical study for flame deflector design of a space launch vehicle.Advances in Space Research, 2017; 59(7): 1833-1847.
18. Aims and Scope.International Journal of Fluid Engineering,2024;1(02):3.
19. Dressler G. Summary of deep throttling rocket engines with emphasis on Apollo LMDE//42nd AIAA/ASME/SAE/ASEE Joint Propulsion Conference & Exhibit. 2006; 5220.
20. Wang Shikai, He Yanfeng, Guo Erpeng, et al. Simulation of Development Effects and Correlation Analysis of Influencing Factors for Multicomponent Thermal Fluids. Journal of Changzhou University (Natural Science Edition),2024;36(03):18-25.
21. Cheng P, Li Q, Kang Z, et al. Combustion dynamics of an extreme fuel-rich throttleable rocket engine during continuously throttling process.Combustion Science and Technology, 2017; 189(4): 717-731.
22. Cui P. Analysis of influence factors on performances for divergent RBCC engine under the flight condition of Ma3, 21st AIAA Int//Space Planes and Hypersonics Technologies Conf.AIAA 2017. 2017; 2178: 6-9.
23. Dong Z, Sun M, Wang Z, et al. Survey on key techniques of rocket-based combined-cycle engine in ejector mode. Acta Astronautica, 2019; 164: 51-68.
24. Cheng P, Li Q, Chen H, et al. Study on the dynamic response of a pressure swirl injector to ramp variation of mass flow rate. Acta Astronautica, 2018; 152: 449-457.
25. Welton D, Bensky M, Hiland J. Variable-Thrust Liquid Propellant Rocket Engines//Summer Meeting. 1963; 268.
26. Giuliano V, Leonard T, Adamski W, et al. CECE: A deep throttling demonstrator cryogenic engine for NASA's lunar lander//43rd AIAA/ASME/SAE/ASEE Joint Propulsion Conference & Exhibit. 2007;5480.
27. Morehead R. Project morpheus main engine development and preliminary flight testing//47th AIAA/ASME/SAE/ASEE Joint Propulsion Conference & Exhibit. 2011;

5927.

28. Olansen J B, Munday S, Devolites J, et al. Project Morpheus: Lessons learned in lander technology development//AIAA SPACE 2013 Conference and Exposition. 2013;5310.
29. Melcher J C, Morehead R L. Combustion stability characteristics of the project morpheus liquid oxygen/liquid methane main engine//50th AIAA/ASME/SAE/ASEE Joint Propulsion Conference. 2014; 3681.
30. Wang P, Wang P, Fan E. Neural network optimization method and its application in information processing. Mathematical Problems in Engineering, 2021; 2021(1): 6665703.
31. Salgotra R, Singh U, Saha S, et al. Self adaptive cuckoo search: analysis and experimentation. Swarm Evol Comput 60: 100751[EB/OL].(2021)
32. Zhou Z, Zhao C, Lu C, et al. Numerical studies on four-engine rocket exhaust plume im**ing on flame deflectors with afterburning. Defence Technology, 2021;17(4): 1207-1216.
33. Saito M, Ohno Y, Kato H, et al. Numerical Prediction of the Spontaneous Ignition of Cool Flame for the Microgravity Experiment by Using Sounding Rocket. TRANSACTIONS OF THE JAPAN SOCIETY FOR AERONAUTICAL AND SPACE SCIENCES, AEROSPACE TECHNOLOGY JAPAN, 2021; 19(4): 539-544.
34. Son M, Lee K, Koo J. Characteristics of anchoring locations and angles for GOX/GCH4 flames of an annular pintle injector. Acta Astronautica, 2020; 177: 707-713.
35. Laurent C, Staffelbach G, Nicoud F, et al. Heat-release dynamics in a doubly-transcritical LO2/LCH4 cryogenic coaxial jet flame subjected to fuel inflow acoustic modulation. Proceedings of the Combustion Institute, 2021; 38(4): 6375-6383.
36. Makhviladze G M, Shamshin A V, Yakush S E, et al. Experimental and numerical study of transient compartment fires. Combustion, Explosion and Shock Waves, 2006; 42: 723-730.
37. Zachl A, Buchmayr M, Gruber J, et al. Shifting of the flame front in a small-scale commercial downdraft gasifier by water injection and exhaust gas recirculation. Fuel, 2021; 303: 121297.
38. Teng Yao, Gong Qingtao, Liu Zhigang, et al. Numerical Simulation of Four-Engine Carrier Rocket Exhaust under Sea Thermal Launch Mode. China Offshore Platform., 2023;38 (04): 68-72.